BRNO UNIVERSITY OF TECHNOLOGY

VYSOKÉ UČENÍ TECHNICKÉ V BRNĚ

FACULTY OF MECHANICAL ENGINEERING
INSTITUTE OF MATERIALS SCIENCE AND ENGINEERING

FAKULTA STROJNÍHO INŽENÝRSTVÍ

ÚSTAV MATEIÁLOVÝCH VĚD A INŽENÝRSTVÍ

EARLY STAGES OF FATIGUE DAMAGE OF STEEL FOR FUSION ENERGETIC

POČÁTEČNÍ STÁDIA ÚNAVOVÉHO POŠKOZENÍ U OCELÍ PRO FÚZNÍ ENERGETIKU

DOCTORAL THESIS – SHORTENED VERSION

DIZERTAČNÍ PRÁCE

AUTHOR   Ing. IVO KUBĚNA

AUTOR

SUPERVISOR   prof. Mgr. TOMÁŠ KRUML CSc.

VEDOUCÍ PRÁCE

SUPERVISOR SPECIALIST   doc. Ing. LIBOR PANTĚLEJEV PhD.

VEDOUCÍ PRÁCE - SPECIALISTA

BRNO 2012

Key words: low cycle fatigue, ODS steels, surface relief evolution, small crack growth rate, fatigue life estimation.

Klíčová slova: nízkocyklová únava, ODS oceli, vývoj povrchového reliéfu, rychlost únavových trhlin, odhad únavové životnosti.

Institute of Material Science and Engineering
Faculty of Mechanical Engineering
University of Technology Brno

kubena@ipm.cz

Contents

1 Introduction

Fossil fuel is going to be exhausted and its massive usage has very negative environmental effects, thus it is necessary to look for new sources of electrical power. One of the promising sources of electrical energy is the thermonuclear fusion. It is the same reaction as running on the Sun and thanks to this energy life on the Earth can exist. This technology appears to be the environmentally friendly because products created by fusion reaction do not include harmful components such as CO_2 and NO_2 which are produced in thermal power plants.

The commercial use of fusion energy as a source of electric energy is a main goal of world-wide cooperation coordinated in Europe by EFDA (European Fusion Development Agreement). This work is a part of this cooperation focusing on fatigue behaviour of newly developed steels. An experimental reactor ITER (International Thermonuclear Experimental Reactor) is under construction in Cadarache in France. According to the actual schedule, the first experiment in ITER should be performed in 2020 [1]. It is expected that most of physical, technical and material problems will be studied and solved during ITER service. Next planned experimental reactor DEMO could be very similar to the commercial power plants and it should run with continuous fusion reaction with performance of 2 GW [2].

The selection of a structural material for future fusion power plant is one of the most critical issues. Structural materials will be exposed to very intense neutron irradiation originating from the plasma reaction. These neutrons will create damage in materials, e.g. displacement cascades, transmutation products and helium production. Theoretical calculations as well as irradiation experiments with neutrons of high energy (like during fusion reaction) are necessary. A finalisation of the IFMIF (International Fusion Materials Irradiation Facility) is a necessity for such experiments [3]. Structural materials must have good physical properties in combination with high irradiation resistance, low residual activation, low swelling and good compatibility with cooling media. Moreover, for achievement of high thermal efficiency the reactor must be operating at temperature as high as possible [4].

The RAFM (Reduced Activation Feritic/Martensitic) and RAF (Reduced Activation Ferritic) steels are the most promising candidates for structural material for future fusion reactor. Their advantages are lower thermal expansion coefficient and better resistance against swelling in comparison with austenitic stainless steels. Maximum operating temperature of RAFM steels is of about 550 ℃ [5].

Recently, RAFM steels prepared by powder metalurgy with dispersion of fine yttrium oxides were proposed for some parts of the reactor. Oxide dispersion was supposed to increase operating temperature, to stabilise microstructure at elevated temperatures and to suppress cyclic softening which was observed by many authors in RAFM steels, see e.g. [6, 7]. Mechanical properties of ODS steels were widely studied [8, 9, 10, 11]. It was documented that oxide dispersion increases operating temperature to 650 ℃ in the ODS Eurofer steel [12] and to 750 ℃ in case of ferritic ODS steels [13]. Information about fatigue properties of ODS steels are rare in literature. Ukai et al. measured stable cyclic behaviour in the 9Cr and 12Cr ODS steels [14]. This work brings complex description of fatigue behaviour of three ODS steels.

2 Main goals of the thesis

This work is focused on fatigue properties of three ODS steels for fusion energy. Main goals can be specified as:

- Determination of basic fatigue life curves, Coffin–Manson and Wöhler curves at room and elevated temperatures.
- Determination of cyclic hardening/softening curves at room and elevated temperatures.
- Specimen surfaces observation for detection of short crack initiation sites.
- Measurement of fatigue crack growth rate.
- Transmission electron microscopy observation for determination of microstructure evolution due to cyclic deformation.
- Explanation of fatigue behaviour of studied ODS steel in relation to the microstructure.

3 Experiment

3.1 Materials

In this work, fatigue properties of three steels strengthened by fine oxide dispersion (ODS) are studied. These materials are produced by powder metallurgy in small quantity. The chemical composition of these steels is shown in table 1. All materials contain the same amount of Y_2O_3 particles and belong to group of materials with reduced activation.

The **ODS Eurofer steel** batch used in this study was produced by *Plansee Holding AG* in the form of a hot rolled plates, with a final thickness of 17 mm. Yttrium was added in a form of fine oxide particles. The chemical composition of this material is given in table 1. The final heat-treatment applied to the material was: annealing at 1100 ℃ for 30 min, air-cooling, tempering at 750 ℃ for 2 hours, air cooling. The material was supplied as a block of $16 \times 32 \times 45$ mm. Twenty and twelve specimens were prepared in longitudinal (L) and transverse direction (T), respectively.

The first variant of 14Cr ODS ferritic steel studied in this work was finalised in **the CEA** (Commissariat à l'énergie atomique, Saclay, France) in 2008. The first step, the preparation of a metal powder and an yttrium powder was performed by the Austrian company *Plansee Holding AG*. In the CEA, the resulting powder was degassed at 300 ℃ and consolidated by hot extrusion at 1100 ℃, air-cooled and then annealed at 1050 ℃ for 1 hour. The chemical composition is given in table 1. This variant of ferritic steel is called simply "CEA steel" in following parts of this work. The material was supplied as a cylinder with diameter of 15 mm with length of 29 mm, 8 specimens parallel to the extrusion direction were prepared. These specimens were used for study of cyclic stress – strain response and of number of cycles to failure at RT, 650 ℃ and 750 ℃.

Table 1: Chemical composition of studied steels in wt. %

material signed as:	Cr	W	Ti	Mn	V	Ta	C	O	Y_2O_3	Fe
Eurofer ODS	8.9	1.1	-	0.47	0.2	0.081	0.11	0.201	0.3	rest
the CEA steel	13.65	1.17	0.3	0.33	-	-	0.05	0.06	0.3	rest
the EPFL steel	14	2	0.3	-	-	-	0.067	0.38	0.3	rest

Bigger batch of this material was supplied in year 2010. It was possible to prepare sixteen specimens (also parallel with stress axis). Half of them was used for fatigue test at RT and second half was used for small fatigue crack growth measurement.

The second variant of 14Cr ODS ferritic steel studied in this work was produced at **the EPFL** (École Polytechnique Fédérale de Laussane, Switzerland). The powder was prepared by planetary ball milling for 50 hours in H_2. The heat treatment consisted of degassing at 800 ℃ for two hours following by a HIP at 1150 ℃ and 200 MPa and of annealing at 900 ℃. The chemical composition is given in table 1. This variant of ferritic steel is called simply "EPFL steel" in following parts of this work. The material was supplied as a block of $20 \times 20 \times 28$ mm. 16 specimens were prepared.

3.2 Standard fatigue tests

Due to limited amount of material produced by powder metallurgy and in order to maximise the number of the specimens, small specimens were prepared according to the design developed within the framework of the "Small Specimen Testing Technology" program [15]. These specimens had a diameter of 2 mm and a gauge length of 7.6 mm and they were used for pure fatigue tests, see fig. 1. Inconel "holders" were used for fixing of specimens to the grips of fatigue machine. This kind of geometry was used for the EPFL steel, the ODS Eurofer steel and the CEA steel supplied in 2008. Slightly different geometry was used for batch supplied from the CEA in 2010. Diameter of specimens was extended to 2.3 mm as well as gauge length to 9 mm. Gauge length of all tested specimens was mechanically and electrolytically polished.
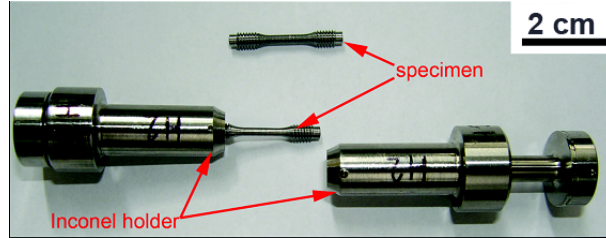
Figure 1: Specimen and Inconel grips

The specimens were cycled in MTS 880 servohydraulic machine controlled by the MTS FlexTest electronics. The fatigue tests were performed in symmetrical cycle with constant strain amplitude ε_a (R_ε = -1). The controlling electronic was adjusted to minimised specimen geometry very well and strain amplitude was kept constant precisely during tests. Force was measured by a load cell and displacement by an extensometer with ceramic rods attached to the specimen gauge length, see figure 2. Strain rate equal to $2 \times \tilde{1}0^{-3}$ s^{-1} was kept constant during cycling. Room temperature (RT) in laboratory was kept constant (23 ℃) during testing. This arrangement is also applicable for testing at elevated temperatures, because the measuring part of the extensometer is placed outside of a furnace. The specimen heating is reached using three-zone furnace. Temperature in each zone was controlled by a thermocouple attached to grips and fourth thermocouple was attached on the specimen. Grips were cooled by a water circuit. Force and displacement

were recorded during cycling. Subsequently, they were recalculated to engineering stress and strain. Plastic strain amplitude was determined as half-width of hysteresis loop.
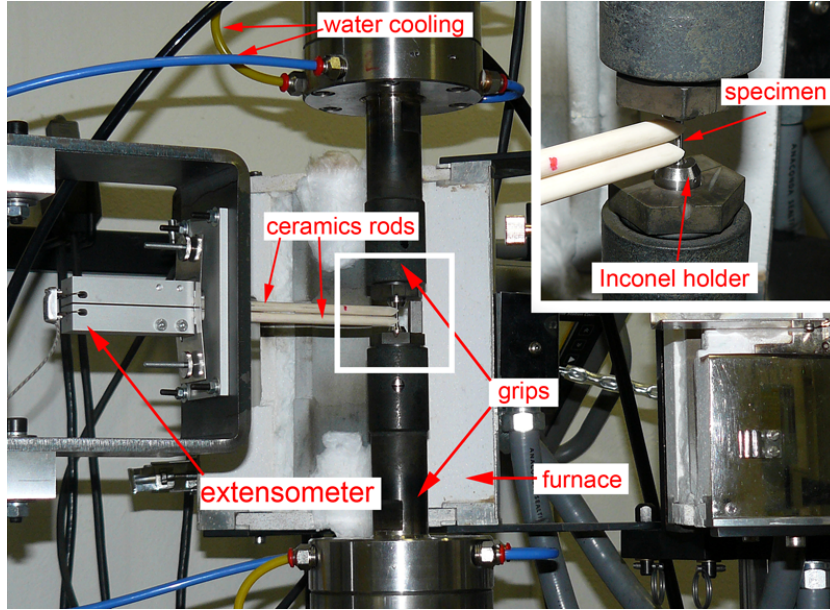
Figure 2: Experimental arrangement allowing experiments at room and elevated temperatures. Attachment of ceramic rods on specimen is show in detail

3.3   Small crack growth measurement

Kinetics of small fatigue crack growth was measured in the CEA steel and in the ODS Eurofer steel. It was not possible to measure it in the EPFL steel, because of lack of supplied material.

The geometry described in previous section was used. Moreover, the shallow notch was fabricated on gauge length. The notch surface was polished mechanically, electrolytically and in some cases the final polishing was performed using 0.25 μm diamond paste. This notch causes stress concentration which is sufficient for initiation of main crack in this area. Typically, only one crack initiated in the CEA steel, which was found out during surface observation of specimen after failure, see section 4.4. Therefore, pre–cracks were prepared in polished area using focused ion beam (FIB) technique to ensure that the crack will propagate in observed area. Parameters of ion beam were set to prepare a crack perpendicular to the stress axis of length 30 or 50 μm with semicircular depth profile in both studied materials.

The fatigue tests were regularly interrupted and two pre–cracks were photographed by a light microscope with long focal distance, which was attached to the machine frame. Micrographs were subsequently analysed and a dependence of crack length on number of cycles was obtained. The crack length a was defined as half length of the surface crack length projected into the direction perpendicular to the specimen axis.

4 Selected results

Results achieved in this work are briefly presented in this chapter. It contains of i) description of microstructure of studied materials in as – received and fatigued state; ii) cyclic hardening/softening curves, cyclic stress–strain curves and the fatigue life curves which were determined at room temperature, 650 and 750 °C; iii) SEM observation of specimen surface after fatigue loading in all studied steels; iv) small fatigue crack growth rate measurements in the ODS Eurofer steel and the CEA steel.
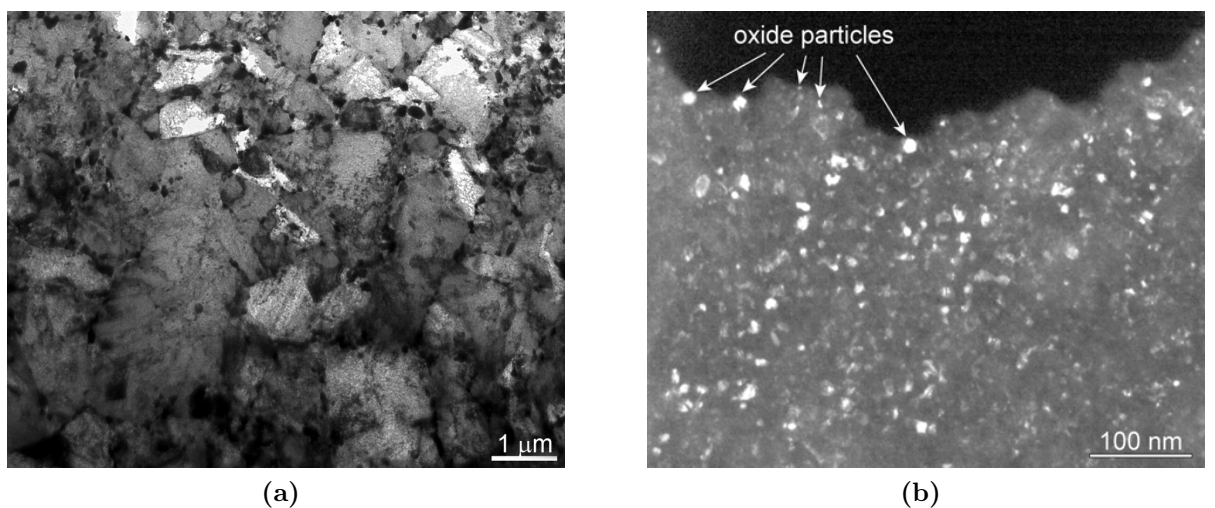
4.1 Microstructure

4.1.1 As–received state

Observations revealed a fine microstructure in all cases. Oxides particles can be seen only in TEM dark field mode, an example is shown in figure 3b. The amount and the mean size of oxides is the same for all materials, nevertheless not much is known about the homogeneity of oxide particles distribution. Since it is experimentally difficult to assess the distribution of nanometric particles in the macroscopic sample, it cannot be excluded that the quality of powder mixing was different for the three materials. Some differences in microstructure among studied materials, especially in grain size and geometry, were found.

Majority of the volume of the ODS Eurofer steel is filled by approximately equiaxed grains/ subgrains (figure 3a). At some place, elongated rests of tempered martensitic laths are visible. The thickness of the laths is about 500–700 nm. Dislocations are present in high density. Grain boundaries are decorated by carbides of typical dimension of 100 nm.

The equiaxed grains with the average size of 0.49 μm $\pm$ 0.2 μm were determined from TEM micrographs of the microstructure of the CEA steel in section perpendicular to the extrusion axis. Grains are elongated in extrusion direction. The dislocation density in

(a)   (b)

Figure 3: Microstructure of the ODS Eurofer steel: a) martenisitic laths and carbides (TEM - bright field); b) fine oxide particles (TEM - dark field)

grains is relatively high. An example of TEM micrograph is shown in figure 4a. The bimodal grain size distribution was found in the EPFL steel. The microstructure is consisted of small grains with the average size of 0.34 μm $\pm$ 0.18 μm and of big grains with size of several micrometers. The dislocation density in both grains types is high. Both type of grains are shown in figure 4b.
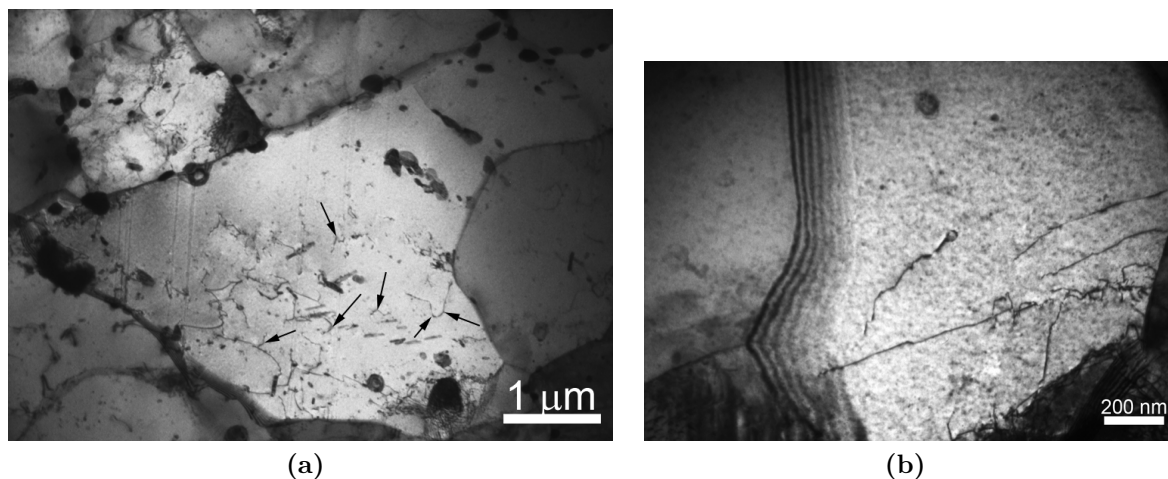

(a)   (b)
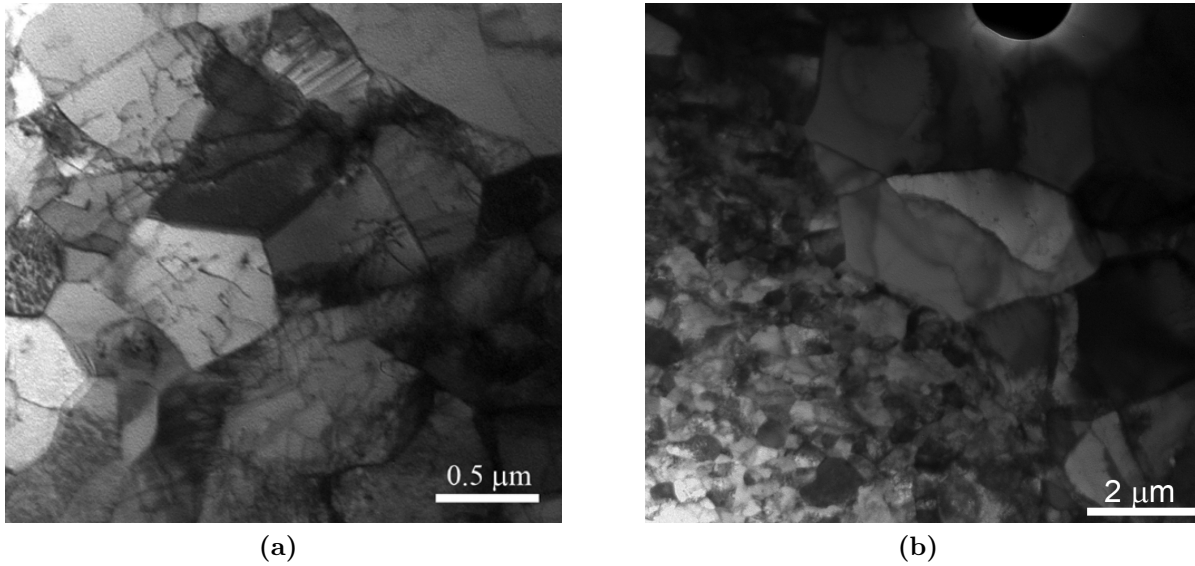
Figure 4: Microstructure of 14Cr ODS ferritic steels: a) the CEA steel; b) the EPFL steel

4.1.2 Fatigued state

The ODS Eurofer steel
Fatigue loading caused some changes in microstructure comparing with the as – received

(a)   (b)

Figure 5: TEM micrographs of the ODS Eurofer steel after fatigue loading: a) at 650 ℃, bigger grain with high dislocation density, dislocations are pinned by oxide particles; b) at 750 ℃, a detail of grains with dislocations pinned by oxide dispersion

10

state. Overall dislocation density decreased, some of grains were found to be almost dislocation free. Individual dislocations were found. Low angle boundaries build by dislocations were observed. Some grains increased, it means that cyclic plastic deformation can destroy weak low angle boundaries even in material strengthened by oxide dispersion. Carbides are situated at the grain boundaries, no changes in carbide distribution and in their size were observed.

At elevated temperatures, overall dislocation density decreased too. Some low angle boundaries were destroyed by cyclic plastic deformation leading to growth of grains size as well as at RT. The grain size varies from 1 μm to several micrometres. Two types of bigger grains were observed: dislocation free grains and grains with high dislocation density (figure 5a). The effect of oxide dispersion (dislocations are pinned by oxides) is clearly visible and marked by arrows in figures 5a. Another detail of grain found in specimen cycled at 750 ℃ is presented in figure 5b. Obviously, the oxide dispersion plays important role even at such high temperatures for steels.

The CEA steel
The microstructure of the CEA steel cycled at RT does not exhibit any substantial changes. The dislocation density inside grains slightly decreased, but no more differences were not found comparing the as – received state. The statistical analysis revealed grains size of 0.5 ± 0.15 μm in section perpendicular to the extrusion axis, i.e. no difference with as – received state. This fact is consistent with stable cyclic behaviour of the CEA steel at RT. The elongated microstructure in the section parallel to the extrusion axis is shown in figure 6a.

Some changes in microstructure due to fatigue loading were identified in specimens cycled at 650 ℃. Statistical analysis was carried out in order to determine grain size distribution. In spite of the fact that a few grains of size around 1 μm are present the in

(a) (b)

Figure 6: TEM micrographs of the CEA steel after fatigue loading: a) at RT, an elongated structure in extrusion direction; b) at 650 ℃, grains with high dislocation density with marked tilt and twist LAB

11

microstructure, the grain size was measured as 0.53 ± 0.23 μm in section perpendicular to the extrusion axis. It can be concluded that grain size increasing is statistically negligible. The dislocation density inside grains is quite high. Dislocation are pinned by oxides. An example of the tilt low angle boundary is marked by arrow in left part of figure 6b and the twist low angle boundary is marked right part of figure 6b.

The EPFL steel

The regions of smaller grains are not affected significantly by fatigue loading at RT in the EPFL steel. Grain size in these regions remains constant, which was proved by statistical analysis, only the dislocation density slightly decreased. The grain size in regions of bigger grains varies from 1 μm to 3 μm, which is also comparable with as–received state. Two types of bigger grains were found after fatigue loading at RT. The first type of grains possesses very high dislocation density. Dislocations in such grains are pinned by oxide particles. The second type of bigger grains is shown in figure 7a. The interior of grains is usually fractionated to small subgrains. Individual dislocations are also present in subgrains. The first type of grains is more frequent in microstructure.

At elevated temperatures, grain size of small grains was not changed during fatigue loading. Dislocation density inside small grains is lower in comparison with as – received state and specimens cycled at RT. Various bigger grains were found in microstructure. Grains with lower dislocation density, grains almost dislocation free and grains with very high dislocation density ($\rho \doteq 1.7 \times 10^{14}$ m^{-2}), see figure 7b. The dislocation are pinned by oxide dispersion. No 3-D dislocation patterns were found in microstructure as well as in the ODS Eurofer steel and the CEA steel.


(a)   (b)
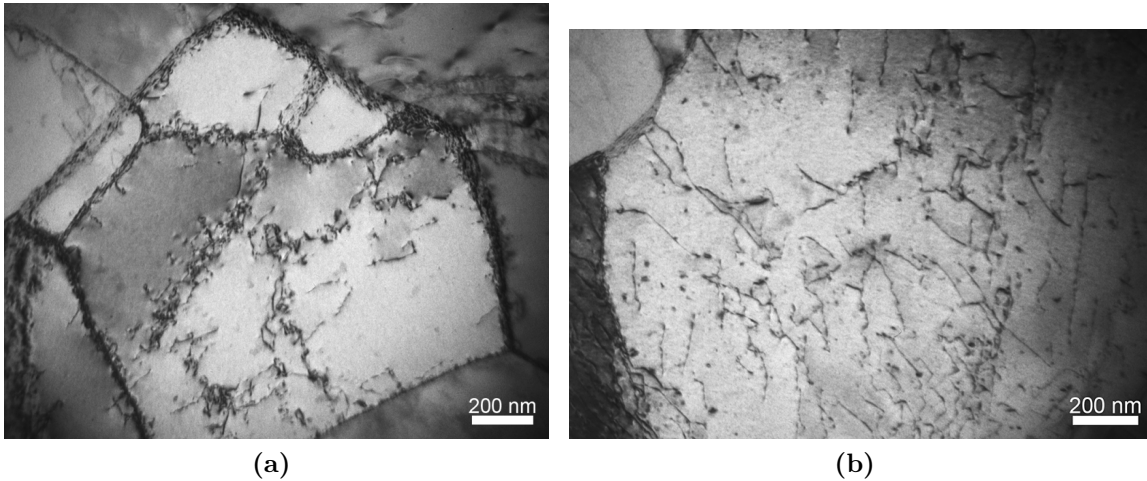
Figure 7: TEM micrographs of the EPFL steel after fatigue loading, a) at RT, bigger fractionated into subgrains by LAB boundaries; b) at 650 ℃, bigger grain with very high dislocation density, dislocations pinned by oxide dispersion

4.2 Cyclic hardening/softening curves

The stress-strain data in selected cycles were stored during cycling allowing plot of individual hysteresis loops and subsequent determination of cyclic hardening/softening curves. The tests were performed in constant total strain amplitude mode, therefore cyclic hardening/softening curves were obtained in two representation, specifically in $\sigma_a = f(N)$ and in $\varepsilon_{ap} = f(N)$ representations. Representative values of σ_a and ε_{ap} were chosen at the half-life.

Cyclic softening curves of all studied materials and of the Eurofer 97 steel at RT are
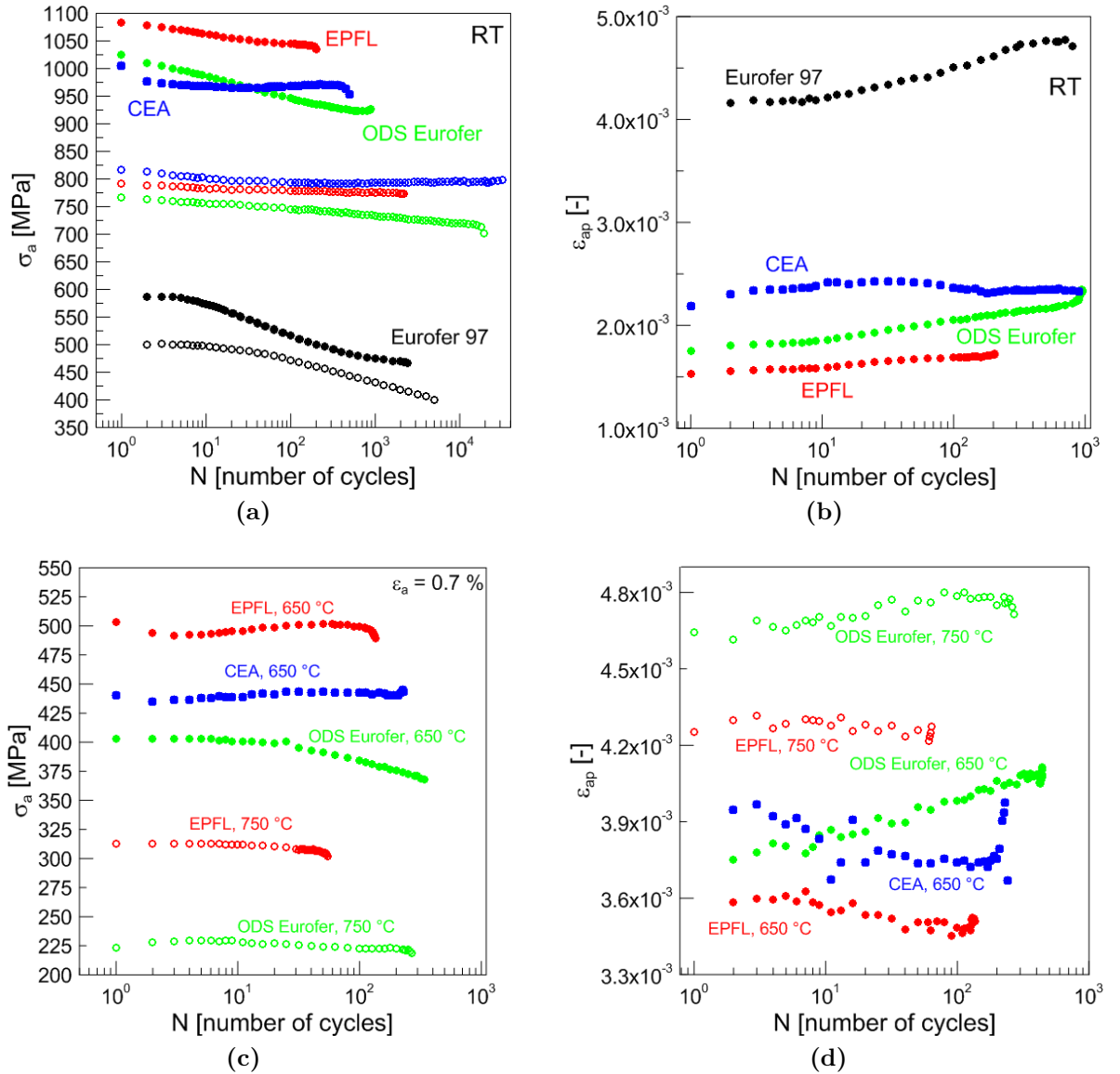
Figure 8: Cyclic softening curves: a) in $\sigma_a = f(N)$ representation at room temperature (full symbols - $\varepsilon_a = 0.7$ %, open symbols $\varepsilon_a = 0.4$ %); b) in $\varepsilon_{ap} = f(N)$ representation at room temperature, $\varepsilon_a = 0.7$ %; c) in $\sigma = f(N)$ representation at elevated temperatures (full symbols - 650 °C, open symbols - 750 °C); d) in $\varepsilon_{ap} = f(N)$ representation at elevated temperatures

13

plotted in both representations in figures 8a and 8b. The strengthening effect of oxide dispersion is obvious, stress levels are almost doubled comparing non – ODS with ODS steels. Moreover, cyclic softening is suppressed by oxides but it still persists for some experimental conditions especially in the ODS Eurofer steel. The EPFL steel possesses the highest strength for the highest strain amplitude. The strength of ODS ferritic steel is very similar under loading with medium strain amplitude, while the ODS Eurofer steel possesses the lowest strength among studied ODS steels in this amplitude region (see open symbols in figure 8a).

Comparison of σ_a and ε_{ap} evolution with number of cycles at elevated temperatures is shown in figure 8c and 8d. All studied steels keep quite high strength at 650 ℃ in comparison with conventional non – ODS RAFM or RAF steels, see e.g. [16]. The EPFL steel cyclically resists to stress higher than 300 MPa even at 750 ℃. Unfortunately, the failure of specimens from the EPFL steel occur after the lowest number of cycles at all tested temperatures. Strength of ferritic steels is higher than that of the ODS Eurofer steel at all testing temperatures. Due to the lack of material, no experiments were done with the CEA steel at 750 ℃.

4.3   Fatigue life curves

The derived[1] Wöhler plots of all materials obtained at RT are shown in figure 9a. The important improvement of strength in comparison with Eurofer 97 steel due to oxide dispersion is documented. The stress amplitude for half-life at a given N_F is almost doubled for all studied ODS steels comparing with the Eurofer 97 steel. The ODS Eurofer steel and the EPFL steel curves have a similar slope, nevertheless the stress levels are

---

[1]Because σ_a is not constant during the test and σ_a at the half life is used, the adjective "derived" is used.
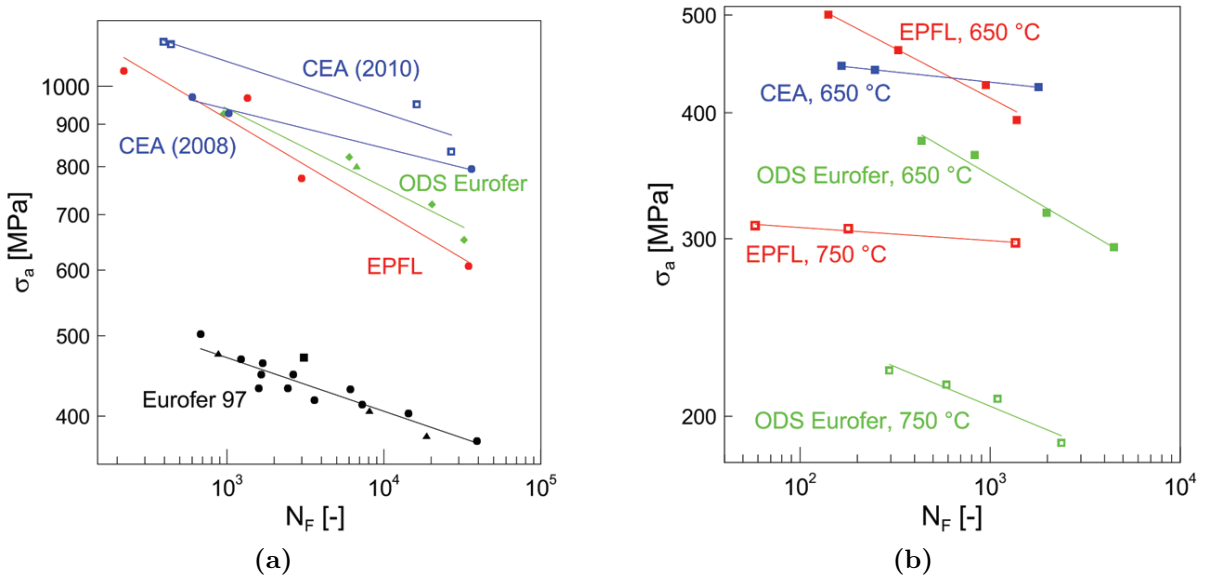

Figure 9: Derived Wöhler curves; a) RT; b) elevated temperatures: full symbols - 650 ℃; open symbols - 750 ℃

14

higher for the EPFL steel than for the ODS Eurofer steel. On the other hand, fatigue life is longer for the ODS Eurofer steel than for the EPFL steel at the same total strain amplitude σ_a. There is no visible difference in N_F of specimens with T and L axis direction in the ODS Eurofer steel. The CEA steel (2010) curve lie above all others curves meaning the longest fatigue life of all studied materials. The batch of the CEA steel obtained in year 2008 exhibits lower strength than batch from year 2010.

At 650 ℃, the stress levels for all ODS materials are still relatively high, see the derived Wöhler plot in figure 9b. Both ferritic steels exhibits higher cyclic strength than the ODS Eurofer steel. The highest stress values are obtained for the EPFL steel in high stress amplitude region, whilst the best σ_a response in low strain amplitude region was found in the CEA steel. The ODS Eurofer steel and the EPFL steel keep quite high stress amplitudes even at 750 ℃.

The resistance of the ODS steels and the Eurofer 97 steel to cyclic plastic strain at RT is shown in figure 10a as a Coffin-Manson plot. Apparently, the Eurofer 97 steel shows the best resistance to cyclic plastic deformation, on the contrary the EPFL steel exhibits the lowest resistance to cyclic straining. The ODS Eurofer steel and the CEA steel curves lie almost on the same curve and their resistance to cyclic straining is better in comparison with the EPFL steel. The data measured in CEA steel 2008 and 2010 are distinguished in figure 10a (open symbols – year 2010; full symbols – 2008), and they were fitted adequately by one curve.

Coffin-Manson plots determined at elevated temperatures are shown in figure 10b. The resistance against cyclic plastic deformation is similar at elevated temperatures as at room temperature. The CEA steel exhibits a little lower cyclic plastic strain resistance than at room temperature. The slopes of curves for the EPFL steel are significantly different at 650 ℃ and 750 ℃.
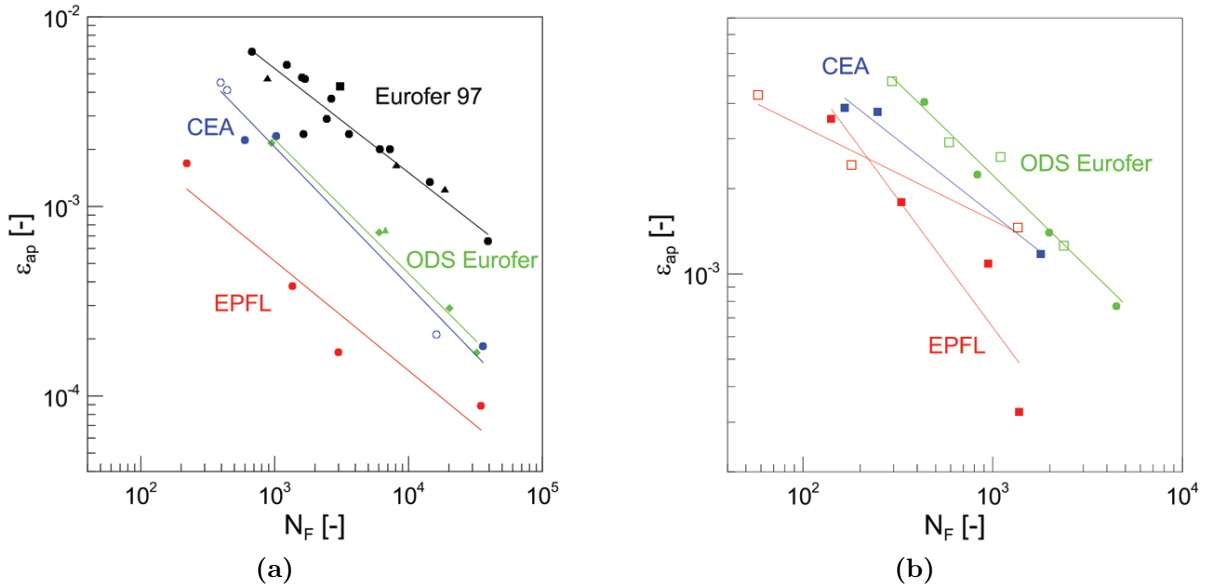

Figure 10: Coffin–Manson curves: a) RT; b) elevated temperatures: full symbols - 650 ℃; open symbols - 750 ℃

15

4.4 Surface relief after fatigue loading and crack initiation sites

4.4.1 ODS Eurofer steel

An example of surface relief formed during fatigue loading is shown in figure 11a. The surface relief is developed in large volumes of similar crystallographic orientations of several microns in size, i.e. in the blocks fractionated into the subgrains. Nevertheless, the relief is not formed in usual way of persistent slip markings of typically 1 μm in thickness but all the surface of such grain is covered by rough, mostly parallel, thin bands. The nucleation of the fatigue cracks takes place inside these surface rough zones or at the interface of these zones and seemingly non–deformed matrix.

Focus ion beam (FIB) technique was used for preparation of thin lamella for TEM exactly from place where the surface relief was formed. The lamella preparation process is well described in the literature [17, 18, 19]. Typically, dimensions of FIB lamellas are 15 μm × 10 μm with thickness of about 75 nm. TEM lamellas were prepared from the ODS Eurofer steel specimen cycled at $\varepsilon_a = 0.7$ %. The TEM micrograph is shown in figure 11b. Grains are visible very well and their size is in agreement with grain size measured in TEM micrographs taken from TEM foils prepared by standard procedure. The surface relief is marked by arrows. Even though the specimen surface is clearly visible (see detail in figure 11b), no arranged dislocation structure was found neither under specimen surface relief nor in TEM foils prepared using standard technique. The typical FIB damage is present in form of small dislocation loops.

(a)   (b)
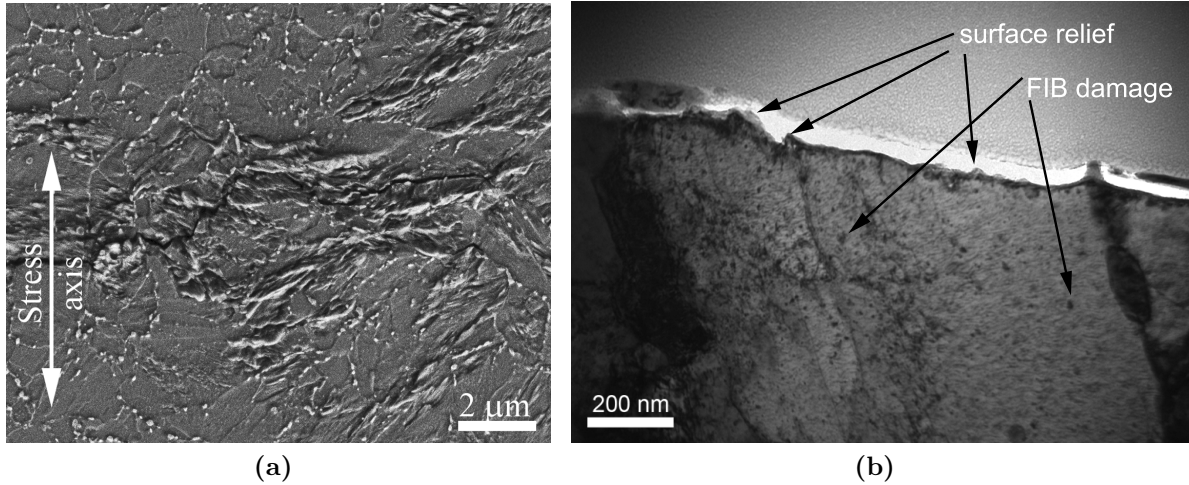
Figure 11: a) Surface relief formed in the ODS Eurofer steel due to fatigue loading at RT; b) TEM micrograph of thin FIB foil prepared from the surface relief

4.4.2 CEA steel

In the case of the CEA steel, SEM observation revealed relatively high density of fatigue cracks in specimens cycled with high strain amplitudes. No clear surface relief (e.g. extrusions, intrusions, roughened surface) formed due to the cyclic straining was observed. An example of a nucleated fatigue crack is shown in figure 12a. Small shear bands

inclined to 45 degrees to the stress axis are visible close to the crack tips. Note the elongated microstructure formed by the hot extrusion. Similar observation was performed on specimens cycled using low strain amplitude. In this case, the density of fatigue cracks is very low. All observed fatigued cracks (all amplitudes) initiated from microstructural defects (voids). Fatigue cracks grew mostly perpendicularly to the stress axis, the growth in "stage I" [20] common to materials having bigger grains was not found.
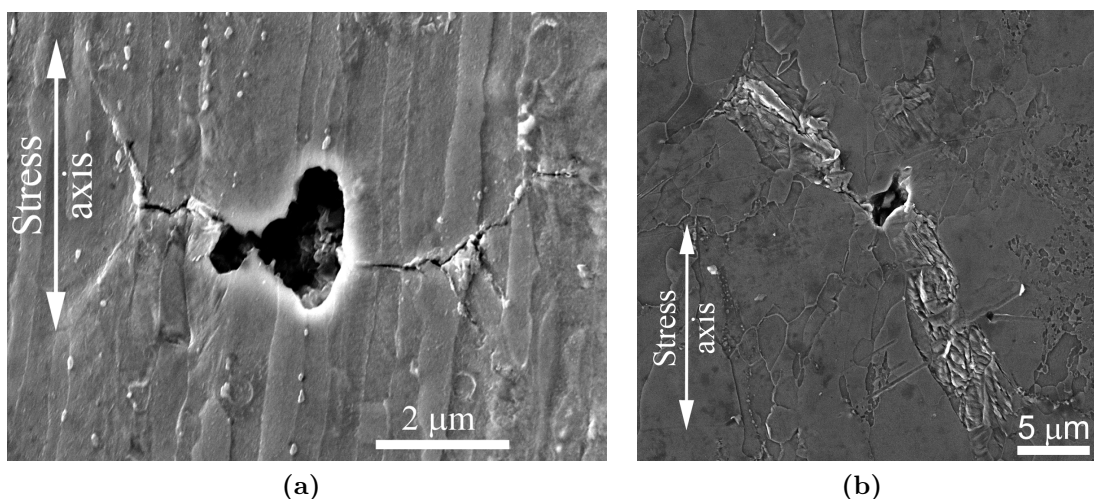
4.4.3 EPFL steel

The situation is quite different in the case of the EPFL steel. The surface relief originated due to cyclic plastic loading is formed in some larger grains 12b. The relief is not formed in usual way of persistent slip markings of typically 1 μm in thickness but all the surface of such grain is covered by rough, mostly parallel, thin bands. The inspection of micrographs reveals that the preferential crack nucleation sites are small voids surrounded by grains with rough surface. Crack nucleation within the surface relief without a void was observed too. The crack pass is most often located along the interface between the rough area and seemingly non-deformed region. Intergranular crack growth is observed in some areas too.
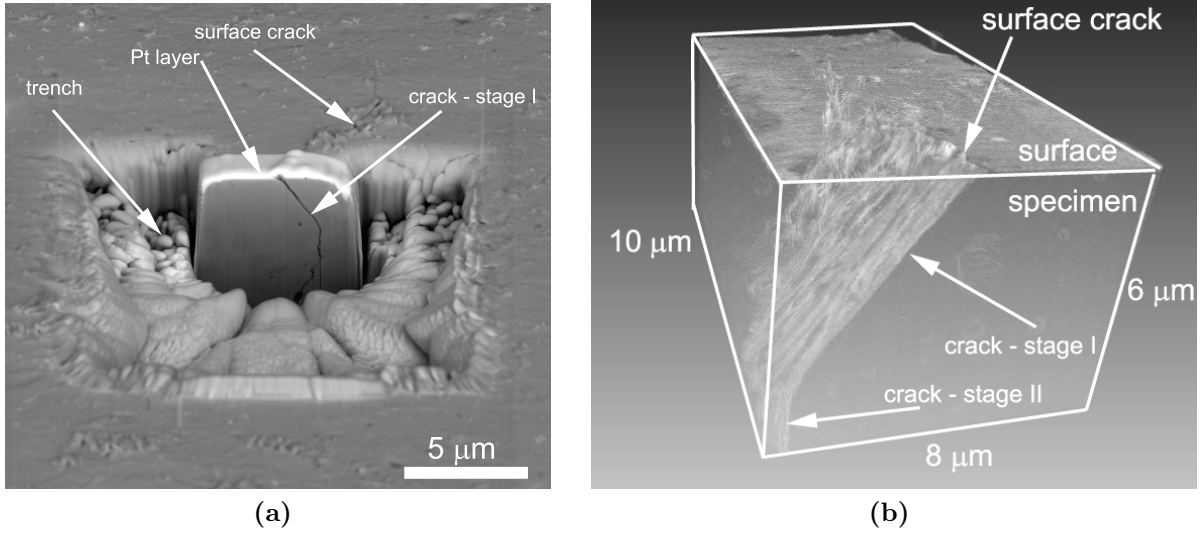
4.5 Small crack growth

4.5.1 Small crack growth path

The small crack growth path under the specimen surface was investigated by means of FIB – SEM 3D tomography in the ODS Eurofer steel. The principle of this methodology and examples of applications in the fatigue crack growth investigations can be found for example in [21, 22, 23, 24] and one of preparation steps is shown in figure 13a. The result of 3D tomography is shown in figure 13b. 3-D micrograph revealed short period of "stage I" propagation. The crack is inclined to 45 degree to the specimen surface only

(a)   (b)

Figure 12: Surface relief formation due to fatigue loading observed in a) the CEA steel; b) the EPFL steel

a few micrometeres in maximum, then crack is turned to perpendicular direction to the specimen surface (stage II of crack propagation).

Figure 13: a) An example of the slice prepared using FIB with marked trenches, Pt protective layer and surface crack; b) 3-D image composed from particular slices with marked growing stages

4.5.2 Small crack growth rate

The small crack growth rate was measured in six specimens from the ODS Eurofer steel and in four specimens from the CEA steel at RT. The measurement was not performed in the EPFL steel, because of the lack of specimens. Examples of light microscopy micrographs are shown in figure 14. Pre–cracks prepared by FIB technique are clearly visible in both cases. Crack started to grow after some initiation period. The crack length is marked in micrographs too.
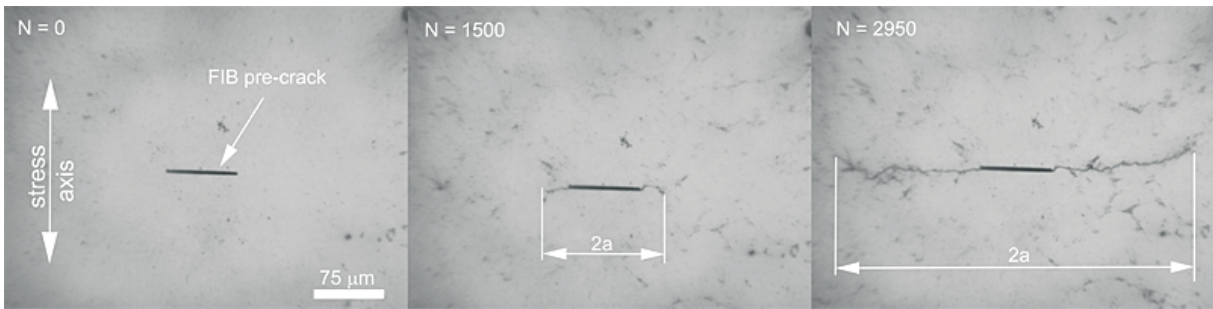
Figure 14: Three light microscopy micrographs taken in different number of cycles N in the ODS Eurofer steel loading with $\varepsilon_a = 0.5$ %

The crack length a was defined as half length of the surface crack length projection into the direction perpendicular to the specimen axis. Crack length was measured in particular intervals during cycling which were adjusted to the crack growth rate to obtain

18

at least twenty pairs of crack length and number of cycles between the onset of cycling and the fracture. An examples of dependence of crack length on number of cycles is shown in figure 15a. The exponential curve matches measured data very well in all cases, which was found for others materials too [25, 26, 27, 28, 29]. Experimental data were fitted by equation $a = a_i \exp(k_g N)$, where a_i and k_g are free parameters which were determined by regression analysis.
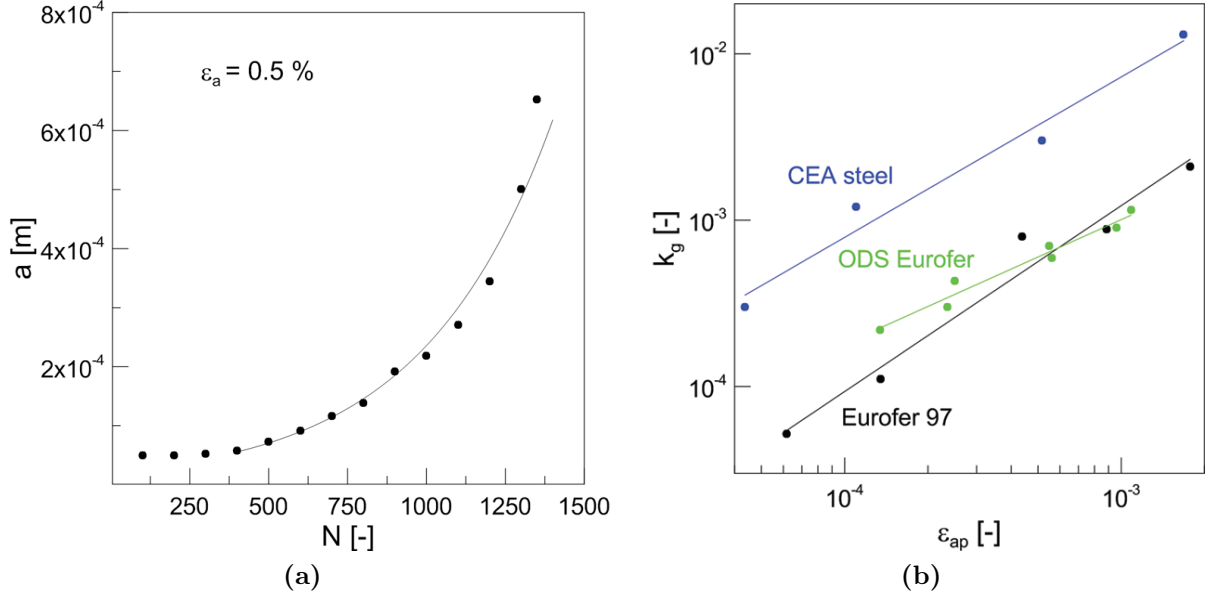
Figure 15: a) An example of the dependence of crack length on number of cycles measured in the CEA steel; b) crack growth coefficient as a function of plastic strain amplitude for the CEA steel, the ODS Eurofer steel and the Eurofer 97 steel

It was proposed by Polak [29] that coefficient k_g is a function of plastic deformation only, $k_g = k_{g0} \, \varepsilon_{ap}^d$. This dependence with a power fit is plotted in figure 15b for the CEA steel and the ODS Eurofer steel. Coefficients k_{g0} and d are materials constant allowing easy description of growing crack. These coefficient were calculated as $k_{g0} = 5.66$ and $d = 0.96$ for the CEA steel and as $k_{g0} = 0.175$ and $d = 0.75$ for the ODS Eurofer steel. According to published data for other steels the value of exponent d was expected to be close to one [25, 26, 27, 29]. This is consistent with results measured in the CEA steel. The comparison of crack growth rate coefficient of both studied ODS steels and of non ODS variant of Eurofer steel is plotted in figure 15b. Obviously, the influence of oxide particles on crack growth coefficient k_g is not strong in case of the Eurofer steel. In spite of the fact that coefficient d varies, values of k_g are similar for both variants of Eurofer steels in studied interval. It seems that fatigue cracks grow faster in the ODS Eurofer steel under lower plastic strain amplitudes than in the Eurofer 97 steel. The crack growth rate coefficient is higher in the CEA steel in order of magnitude than in both variant of the Eurofer steel.

5 Conclusions

The main conclusions can be summarised in following points:

1. Microstructure of as–received state

   • Ultrafine–grained microstructure was revealed in all studied steels. The characteristics of microstructural unit and voids were measured.
   • The matrix of the tempered ferritic–martensitic ODS Eurofer steel consists of decomposed martensitic lath, which are decorated by carbides.
   • The pure ferritic matrix was found in the CEA steel. Equiaxed grains were found in section perpendicular to the extrusion axis, grains are elongated in section parallel to the extrusion axis.
   • The microstructure with bimodal grain size distribution is formed in the purely ferritic EPFL steel.

2. Hardening/softening curves

   • The oxide dispersion strengthens material significantly.
   • Cyclic softening was observed at all testing temperatures in the ODS Eurofer steel. Softening rate increases with increasing strain amplitude and decreasing temperature.
   • The CEA steel exhibits stable behaviour at all testing temperatures, slight cyclic hardening was observed at elevated temperatures.
   • Stable behaviour with exception of the highest amplitude at RT was observed in the EPFL steel.
   • Operating temperature of ODS steels can be increased of about 100 ℃ in comparison with the Eurofer 97 steel.

3. Fatigue behaviour

   • The strengthening effect of oxide particles results in high stress levels in cyclic stress–strain curves. Ferritic–martenistic microstructure is less strength than purely ferritic ones at all testing temperatures.
   • The ODS Eurofer steel and the CEA steel exhibits similar resistance to cyclic plastic straining.
   • The EPFL steel exhibits the highest cyclic strength but the shortest fatigue life among studied ODS steels, especially at RT.

4. Microstructure evolution due to fatigue loading

   • No 3-D dislocation arrangement were formed due to fatigue loading in all studied steels.
   • The overall dislocation density decreased during fatigue loading of the ODS Eurofer steel at all testing temperatures. Grain size increased due to destruction of low angle boundaries by cyclic plastic straining. The mean grain size increases more rapidly at elevated temperatures: the higher temperature, the bigger grains were found in the microstructure. Two types of big grains (dislocation free and with high

dislocation density) were distinguished after fatigue loading at elevated temperatures.

• No significant changes in microstructure were found in the CEA steel after fatigue loading at RT. At 650 °C, some grains grew to the diameter of about 1 μm. Nevertheless, statistical analysis proved that this growth is not statistically important. Dislocation density slightly decreased at both testing temperatures.

• Dislocation density decreased at all testing temperatures in small grains in the EPFL steel. Two types of bigger grains were found in microstructure, the ones with very high dislocation density and the ones almost dislocation free.

5. Surface relief formation and fatigue crack initiation

• The surface relief formation was observed in areas with similar crystallographic orientation in the ODS Eurofer steel. Fatigue crack initiated within surface relief. The surface relief formation facilitates fatigue crack initiation.

• No surface relief was formed in the CEA steel during cycling. Fatigue crack initiated in voids. Some shear bands were observed at the fatigue crack tip.

• The surface of bigger grain were roughened in the EPFL steel. Crack usually initiated at the interface between regions of small and big grains.

6. Small crack growth rate measurement

• The small fatigue crack kinetics was measured in the ODS Eurofer steel and the CEA steel.

• Exponential growth of crack with number of cycles was observed in both steels. It implies fact that crack growth rate is a linear function of crack length.

• Parameters k_{g0} and d were determined.

• The small crack growth rate is the same in the Eurofer 97 steel and in the ODS Eurofer steel. The oxide particles have no influence on fatigue crack growth rate in this case. The fatigue crack growth rate is significantly faster in the CEA steel than in the ODS Eurofer steel.

• Tomkins law and Tanaka–Mura equations were analysed in order to test their validity.

• One parameter linear fracture mechanic was found insufficient for accurate description of growing fatigue crack in the studied steels.

7. Fatigue life in the Coffin–Manson plot

• The shortest fatigue life among studied steels was measured in the EPFL steel. The explanation lies in the surface relief formation which facilitated the fatigue crack initiation and in the fast fatigue crack growth rate in ferritic steels.

• The fatigue life of the CEA steel and the ODS Eurofer steel is almost the same. Nevertheless, the fatigue process is completely different. Fast fatigue crack growth rate is compensated by difficult crack initiation in the CEA steel while relatively short fatigue crack initiation period is compensated by slow rate of fatigue cracks in the ODS Eurofer steel.

References

[1] ITER – the way to new energy [online]. [quoted. 2012-10-01]. Accessible form WWW: http://www.iter.org/default.aspx

[2] LACKNER, K.; et al. Long–term fusion strategy in Europe. *Journal of Nuclear Materials*, 2002, vol. 307–311, p. 10–20.

[3] EHRLICH, K.; MÖSLANG, A. IFMIF – An international fusion materials irradiation facility. *Nuclear Instruments and Methods in Physics Research B*, 1998, vol. 139, p. 72–81.

[4] LÄSNER, R.; et al. Structural materials for DEMO: The EU development, strategy, testing and modelling. *Fusion Engineering and Design*, 2007, vol. 82, p. 511–520.

[5] BALUC, N.; et al. On the potentiality of using ferritic/martensitic steels as structural materials for fusion reactors. *Nuclear Fusion*, 2004, vol. 44, p. 56–61.

[6] MARMY, P.; KRUML, T. Low cycle fatigue of Eurofer 97. *Journal of Nuclear Materials*, 2008, vol. 377, p. 52–58.

[7] FOURNIER, B.; et al. Comparison of various 912 % Cr steels under fatigue and creep–fatigue loadings at high temperature. *Materials Science and Engineering: A*, 2011, vol. 528, p. 6943–6945.

[8] STECKMEYER, A.; et al. Tensile properties and deformation mechanisms of 14Cr ODS ferritic steel. *Journal of Nuclear Materials*, 2010, vol. 405, p. 95–100.

[9] SCHAEUBLIN, R.; et al. Microstructure and mechanical properties of two ODS ferritic/martensitic steels. *Journal of Nuclear Materials*, 2002, vol. 307–311, p. 778–782.

[10] YU, G.; NITA, N.; BALUC, N. Thermal creep behaviour of the Eurofer 97 RAFM steel and two European ODS Eurofer 97 steels. *Fusion Engineering and Design*, 2005, vol. 75–79, p. 1037–1041.

[11] HADRABA, H.; et al. Influence of microstructure on impact properties of 9–18%Cr ODS steels for fusion/fission applications. *Journal of Nuclear Material*, 2011, vol. 411, p. 112–118.

[12] LINDAU, R.; et al. Present development status of Eurofer and ODS–Eurofer for application in blanket concepts. *Fusion Engineering and design*, 2005, vol. 75–79, p. 989–996.

[13] HOELZER, D.; et al. Influence of particle dispersions on the high-temperature strength of ferritic alloys. *Journal of Nuclear Material*, 2007, vol. 367–370, p. 166–172.

[14] UKAI, S.; OHTSUKA, S. Low cycle fatigue properties of ODS ferritic–martensitic steels at high temperatures. *Journal of Nuclear Materials*, 2007, vol. 367–370, p. 234–238.

[15] MÖSLANG, A. Development of creep fatigue specimen and related test technology. in *IFMIF User Meeting, Tokyo, 2000.*

[16] AKTAA, J.; SCHMITT, R. High temperature deformation and damage behavior of RAFM steels under low cycle fatigue loading: Experiments and modeling. *Fusion Engineering and Design*, 2006, vol. 81, p. 2221–2231.

[17] GANNUZZI, L.; STEVIE, F. A review of focused ion beam milling techniques for TEM specimen preparation. *Micron*, 1999, vol. 30, p. 197–204.

[18] LI, J.; MALIS, T.; DIONNE, S. Recent advances in FIBTEM specimen preparation techniques. *Materials Characterization*, 2006, vol. 57, p. 64–70.

[19] CLANCY, M.; POMEROY, M. J.; BELOCHAPKINE, S. Improved FIB milling process for TEM preparation of NiAlPt bulk alloy samples containing residual stress. *Micron*, 2012, vol. 43, p. 627–630.

[20] POLÁK, J. *Cyclic plasticity and low cycle fatigue life of metal.* Prague: Academia, 1991, 315 s.

[21] KUBIS, A.; et al. Focused Ion-beam tomography. *Metallurgical and Materials Transactions*, 2004, vol. 35A, p. 1935–1943.

[22] HOLZAPFEL, C.; et al. Interaction of crack with precipitates and grain boundaries: Understanding crack growth mechanisms through focused ion beam tomography. *Scripta Materialia*, 2007, vol. 56, p. 697–700.

[23] MARX, M.; et al. Interaction of microcracks with selected interfacec: Focused ion beam for systematic crack initiation. *Materials Science and Engineering A*, 2006, vol. 435–436, p. 595–601

[24] MAN, J.; et al. Study of cyclic strain localization and fatigue crack initiation using FIB technique. *International Journal of Fatigue*, 2012, vol. 39, p. 44–53.

[25] KRUML, T.; POLÁK, J. Fatigue cracks in Eurofer 97 steel: Part I. Nucleation and small crack growth kinetics. *Journal of Nuclear Materials*, 2011, vol. 412, p. 2–6.

[26] OBRTLÍK, K.; et al. Short fatigue crack behaviour in 316L stainless steel. *International Journal of Fatigue*, 1997, vol. 19, p. 471–475.

[27] POLÁK, J. Mechanisms and kinetics of the early fatigue damage in crystalline materials. *Materials Science and Engineering: A*, 2007, vol. 468–470, p. 33–39.

[28] JISA, D.; et al. Small fatigue crack growth in aluminium alloy EN-AW 6082/T6. *International Journal of Fatigue*, 2010, vol. 32, p. 1913–1920.

[29] POLÁK, J.; ZEZULKA, P. Short crack growth and fatigue life in austenitic-ferritic duplex stainless steel. *Fatigue and Fracture of Engineering Materialsand Structures*, 2005, vol. 28, p. 923–935.

List of selected publications by Ivo Kuběna

[I] KUBĚNA, I.; KRUML, T. Fatigue properties and crack growth in Eurofer steel. *Materials Engineering*, 2009, vol. 16, 3a, p. 32–36.

[II] KUBĚNA, I.; KRUML, T.; HUTAŘ, P.; NÁHLÍK, L.; SEITL, S.; POLÁK, J. Únavové vlastnosti oceli Eurofer vyvíjené pro fúzní energetiku. In *METAL 2009, Hradec nad Moravicí, CZ, 19-21 May 2010.* Paper no. 136. ISBN 978-80-87294-04-8.

[III] MAN, J.; WEIDNER, A.; KUBĚNA, I.; VYSTAVĚL, T.; SKROTZKI, W.; POLÁK, J.. Application of FIB technique to study of early fatigue damage in polycrystals. *Journal of Physics: Conference Series*, 2010, vol. 240, issue 1, p. 1–4.

[IV] KUBĚNA, I.; KRUML, T.; SPÄTIG, P.; BALUC, N.; OKSIUTA, Z.; PETRENEC, M.; OBRTLÍK, K.; POLÁK, J. Fatigue behaviour of ODS ferritic-martensitic Eurofer steel. *Procedia Engineering*, 2010, vol. 2, p. 717–724.

[V] KRUML, T.; KUBĚNA, I.; POLÁK, J. Fatigue behaviour and surface relief in ODS steels. *Procedia Engineering*, 2011, vol. 10, p. 1685–1690.

[VI] KUBĚNA, I.; KRUML, T.; FOURNIER, B.; POLÁK, J. Low cycle fatigue behaviour of ODS steels for nuclear application. *Key Engineering Materials*, 2011, vol. 465, p. 556–559.

[VII] KUBĚNA, I.; FOURNIER, B.; KRUML, T. Effect of microstructure on low cycle fatigue properties of ODS steels. *Journal of Nuclear Materials*, 2012, vol. 424, p. 101–108. IF = 2.052.

[VIII] MAN, J.; VYSTAVĚL, T.; WEIDNER, A.; KUBĚNA, I.; PETRENEC, M.; KRUML, T.; POLÁK, J. Study of cyclic strain localization and fatigue crack initiation using FIB technique. *International Journal of Fatigue*, 2012, vol. 39, p. 44–53. IF = 1.546.

[IX] KUBĚNA, I.; KRUML, T. Fatigue life and microstructure of ODS steels. *Engineering Fracture Mechanics*, Accepted manuscript, in print. IF = 1.353.

Curriculum vitae

Personal information

Name	Ing. Ivo Kuběna
Date of birth	13.2.1984
Nationality	Czech
Address	Družstevní 5, Blansko, Czech Rep.
E-mail	kubena@ipm.cz

Education

2008–present	Doctoral study, Faculty of Mechanical Engineering, Brno university of technology, specialisation: Material engineering. Dissertation thesis: Early stages of fatigue damage of steels for fusion energetic.
2003–2008	Engineering study, Faculty of Mechanical Engineering, Brno university of technology, specialisation: Material engineering. Diploma thesis: Development of nanofabrication methodology for study of mechanical properties of thin films using focused ion beam.
1999–2003	The Secondary Technical School of Mechanical Engineering, Sokolská 1, Brno, Czech Rep.

Working experiences

2008–present	Institute of Physics of Materials, Brno, Czech Rep.

Activities

- Participation in project of GA AS number 106/09/1954.

- Successfully solved project provided by FEI Company.

- Supervision of seminars during Ph.D study

Experimental skills

- Usage of scanning electron microscopy in combination with focused ion beam.

- Performing of EDS, EBSD analysis.

- Observation with transmission electron microscopy.

- Operating of MTS systems for mechanical testing

Abstract

The main aim of the thesis is to explain fatigue behaviour of the ODS Eurofer steel, 14Cr ODS ferritic steel produced in the CEA (Commissariat à l'énergie atomique, Saclay, France) and 14Cr ODS ferritic steel produced in the EPFL (École Polytechnique Fédérale de Laussane, Switzerland). The results are compared with non–ODS variant of Eurofer steel, if possible. This work is part of a wide collaboration coordinated by the EFDA (European Fusion Development Agreement) on development of structural materials for future fusion reactors.

The following experiments were carried out:
• Standard fatigue experiments were performed at room temperature, at 650 ℃ and at 750 ℃. Cyclic hardening/softening curves, cyclic deformation stress–strain curves, Coffin–Manson curves and Wöhler curves were measured. Detailed analysis of hysteresis loops was performed.
• The microstructure of the as–received state was studied by TEM and compared with the microstructure after fatigue loading in order to reveal microstructural changes due to fatigue loading.
• Surface roughening due to cyclic plastic localisation was observed. Crack initiation sites were detected and the mechanism of crack initiation was analysed.
• Kinetics of small fatigue crack growth was measured.

It was found that fine oxide dispersion strengthens studied materials significantly, reduces cyclic softening and stabilises the microstructure in the whole range of testing temperatures. The maximum application temperature is increased. Significant differences in fatigue life of the ODS steels were found and explained by differences in crack initiation mechanisms and small fatigue crack growth rate.